THE PENNSYLVANIA STATE UNIVERSITY
SCHREYER HONORS COLLEGE

DEPARTMENT OF ENGINEERING SCIENCE AND MECHANICS

THE EFFECTS OF ACTIVE AREA GEOMETRY ON LAMINATED PIEZOELECTRIC ACTUATOR PERFORMANCE

JOSEPH GIORDANO
SPRING 2013

A thesis
submitted in partial fulfillment
of the requirements
for a baccalaureate degree
in Engineering Science with honors in Engineering Science

Reviewed and approved* by the following:

Dr. Joseph Cusumano
Professor of Engineering Science and Mechanics
Thesis Supervisor

Dr. Gary Gray
Associate Professor of Engineering Science and Mechanics
Honors Adviser

Dr. Judith Todd
P.B. Breneman Department Head of Engineering Science and Mechanics
Department Head

* Signatures are on file in the Schreyer Honors College.

ABSTRACT

Developers in the blossoming consumer electronics industry are increasingly using haptics, the communication of information through touch, to enhance their product's appeal. This thesis presents the mathematical model and numerical simulations for a vibrational haptic device, a clamped-clamped laminated piezoelectric beam. The goal of this analysis was to evince design insights for the system, allowing engineers to construct a more effective haptic actuator. The equation of motion and vibrational response of the system were derived using piezoelectric constitutive equations, Hamilton's Principal, the Assumed Modes Method, and Galerkin's Method. The haptic performance of the modeled actuator was evaluated based on the total net reaction force and moment amplitudes produced across a range of driving frequencies. Two cases were chosen for simulation. The first case represented the current actuator design method, a rectangular patch of active piezoelectric material laminated on top of the beam. The second case sought to optimize specific modal responses by tailoring the active piezoelectric area across the length of the beam, creating a modal actuator. Numerical simulations of these two cases show that the modal actuators produce much stronger reaction forces and moments compared to the patch actuators. In fact, using a modal actuator instead of the current patch actuators increased the modal forcing by 17.69 for the first mode. The results of this study clearly show the superiority of modal actuators for haptic design. In addition, the study also shows the power of using mathematical models to uncover important design insights that would not be evident otherwise.

TABLE OF CONTENTS

LIST OF FIGURES

LIST OF TABLES

ACKNOWLEDGEMENTS

I could not have completed this work without the extensive and thoughtful guidance of my Thesis Advisor, Dr. Joseph Cusumano. I am thankful for the time and energy he put into teaching me about dynamics, modeling, and life. I also owe a great deal of thanks to Brian Zellers, my internship mentor at Strategic Polymer Sciences. Thank you for introducing me to the world of piezoelectric design. The practical engineering experience I gained during those months has been invaluable. This thesis is a direct extension of the problems we faced, thank you for providing the motivation behind this work. Lastly, I need to thank my excellent Honors Advisor, Dr. Gary Gray. I vividly remember the whirlwind of chalk, equations, and energy that was your introductory dynamics class. Thank you for showing me how exciting dynamics can be.

Chapter 1

Introduction

1.1. Motivation

Consumer electronics sales have grown tremendously over the past decade. Devices are getting smaller, faster, and more efficient even as consumers expect more from the user experience. One way to improve this user experience is through the use of tactile feedback, or haptics [1]. The goal of this thesis is to improve the haptic performance of a laminated piezoelectric beam in the context of handheld electronic devices. This is accomplished using mathematical modeling and simulation.

The predominant method of haptic feedback used in cellphones today is an Eccentric Rotating Motor (ERM) [2]. It produces vibrations by spinning a misaligned mass. Linear Resonance Actuators (LRA) are also being used in certain devices. These actuators produce vibrations by driving a spring-mass system at resonance. These technologies are limited in the range of haptic information they can transmit in several ways. The ERM has a large time constant and is unable to produce strong vibrations at lower frequencies [3]. The LRA actuators have smaller time constants, but their operation is limited to the resonant range defined by the mass-spring system.

Piezoelectric actuators are now starting to replace the traditional vibrational motors. These actuators are an improvement over the traditional mechanical systems for several reasons; they involve no mechanical parts, can use less energy, and can operate over a larger frequency range. Ceramic piezoelectric are the dominant material used to construct these systems, and major electronics producers are already implementing them in their next generation of products.

Ceramic Piezoelectrics are well established and understood with regards to actuator design, but their brittleness becomes a problem in handheld electronics that can be dropped [2].

Strategic Polymer Sciences, a local State College technology company, is developing a patented polymer-based piezoelectric actuator to compete with the currently dominant ceramic varieties. The design of these actuators is still in the prototyping and exploratory phase. The configuration that has shown the most promise and utility is a clamped-clamped laminated piezoelectric beam. This system consists of a single piezoelectric layer bonded onto a substrate material like aluminum or PVC. Engineers at the company predominantly use expensive and complicated Finite Element Analysis software to predict the behavior of the system. This method is powerful, but requires large amounts of time and effort to set up and run individual analyses. Worse, the applicability of one study to another is not clear, so each new case has to be simulated individually. The goal of this work is to mathematically model a clamped-clamped laminated piezoelectric beam with well-established techniques to identify design insights that are not evident from other types of analysis. These design insights can be applied to most design cases immediately without repeated study, and provide engineers with a more confident "feel" of which design constructions will perform best.

1.2. Piezoelectric Actuators and Previous Work

Piezoelectric actuators are electromechanical systems that require knowledge of material science, continuous system dynamics, and vibrational analysis techniques to investigate effectively. An understanding of the constitutive equations and material parameters for piezoelectrics is the first requirement to build a representative model. This material is well documented in various textbooks and ASME standards. Constitutive equations are used to model

the effects of piezoelectric materials on the larger system. Significant work has gone into the study of these actuators. The most relevant information and previous work is described below.

1.1.1. Piezoelectric Materials

Piezoelectric materials are active materials that display electromechanical coupling and have been the subject of much interest and research over the past half-century. This coupling is described by the direct piezoelectric effect and the inverse piezoelectric effect. The former is the accumulation of charge in the material's crystal structure as the result of external strain. The latter is the opposite; an applied electric field causes internal [4]. In general, piezoelectric sensors and energy harvesters take advantage of the direct piezoelectric effect, while piezoelectric actuators use the inverse piezoelectric effect to generate strain or force. Today, ceramic piezoelectrics like barium titante ($BaTiO_3$) and lead zirconate titante (PZT) are the most commonly used piezoelectric materials for actuators. Piezoelectric polymers like polyvinylidene fluoride (PVDF) are also used, but less established because of their relatively recent discovery [5]. These semi-crystalline polymers combine the high strain potential of plastic materials with piezoelectric coupling. The actuators at the center of this study are constructed with a piezoelectric polymer.

1.1.2. Modal Sensors and Actuators Studied by Moon and Lee

The subject of creating actuators using laminated piezoelectric layers has been researched by several groups. In their study, Moon and Lee propose a theoretical framework and experimental verification for designing laminated piezoelectric modal sensors and actuators [6]. One-dimensional plates were used as the basis for this study. These plates consisted of three layers, a thin metal shim in the middle sandwiched between two oppositely poled piezoelectric

layers. The behavior of the plate was described by modal summation, which sums the product of each modal coordinate and mode shape for the plate. The authors applied the orthogonality of the modes to design mode-specific actuators and sensors. They used a cantilevered plate as a case study. The electrode profile and therefore the active area of the two piezoelectric layers were tailored to match the second derivative of the first and second mode shapes using chemical etching. The second derivative of the mode shapes was negative at some points across the length of the plate. At these points, the active area switched to the oppositely polled piezoelectric layer. This process produces a sensor/actuator pair only effective in a specified modal coordinate. The one-dimensional plate system was tested by driving the plate through a frequency range and measuring the electrical response of the piezoelectric circuit. Both the mode 1 and mode 2 sensors responded to the modes they were designed to measure, but there was also a small signal overflow from the other modal coordinate. This discrepancy was attributed to inaccuracies in the chemical etching process.

This study has several implications for the current work. Most importantly, it lays out the theory behind tailoring the active area of the piezoelectric to only sense a specific vibrational mode. It also suggests alternating the polling direction of the piezoelectric material to account for the sign change in the second derivative of the mode shape. Lastly, it points to chemical etching as the source of modal sensor error.

1.1.3. Distributed Control of Laminated Beams by Aldraihem, Wetherhold, and Singh

Aldraihem, Wetherhold, and Singh described how to use laminated piezoelectric layers to sense and control the vibration of a cantilevered beam with and without a tip mass [7]. The study compared the control models derived from two prominent beam deformation theories, shear-deformable (Timoshenko) and shear-indeformable (Euler-Bernoulli). The equations of motion

and boundary conditions were derived for both types of beams using Hamilton's Principle. A tip mass was included in one case to highlight the differences in performance between a sheer-deformable and sheer-indeformable control model. The authors used a finite element simulation of a five layered cantilever beam to evaluate the two control models. The cantilever beam consisted of an aluminum core with PVF_2 (polymer) and PZT (ceramic) layer pairs on the top and bottom. The PVF_2 layers were used for sensing and the PZT layers were used for actuation. The active area of the piezoelectric layers was not shaped and was constant along the beam's length. In the simulation, the excited beam was damped using the laminated sensor/actuator pairs and the transient response was recorded. Both control models provided asymptotic stability, but it was found that accounting for shear deformations and rotational energy in the beam became important for beam aspect ratios (length/thickness) less than 30. Also, instability was produced when the shear-indeformable model was used to damp a simulated shear-deformable beam with a tip mass. The authors concluded that the higher order Timoshenko model is superior for beams with low aspect ratios and added masses.

The analysis performed in the current work uses the Euler-Bernoulli theory of beam deformation to model beam vibration. The system's aspect ratio was kept intentionally high to avoid inaccuracies in the model discussed by Aldraihem et al. While not covered in this study, adding point or distributed masses to the system is a possible area for future analysis. If masses are added, the Timoshenko deformation theory should be used.

1.3. Problem Definition

Unlike the studies outlined above, the basis for this investigation is a clamped-clamped, single-laminated piezoelectric beam. The center of the beam is a thin substrate material such as aluminum or PVC plastic. The single piezoelectric layer laminated on top has a specified active

area dictated by the electrodes. The width of the electrode profile is modeled as a function along the beam's length. This model reflects the current actuator design method at Strategic Polymer Sciences and provides the most applicable insight into the design process.

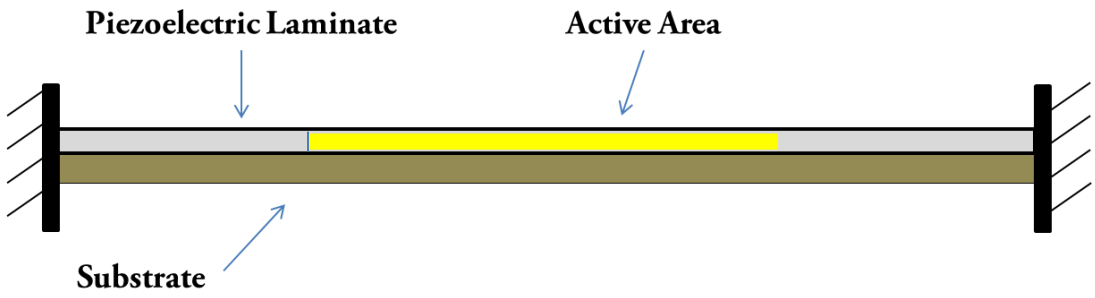

Figure 1: Basic construction of the model for a piezoelectric beam actuator. The beam consists of a substrate layer, laminated piezoelectric layer, and a specific active area defined by the electrodes.

When an electric field is applied to the active area of the piezoelectric, the material produces strain through the inverse piezoelectric effect. If the voltage is cycled harmonically, the beam will vibrate. The desired vibration is transferred from the system to the user through the clamped boundary conditions at both ends of the beam.

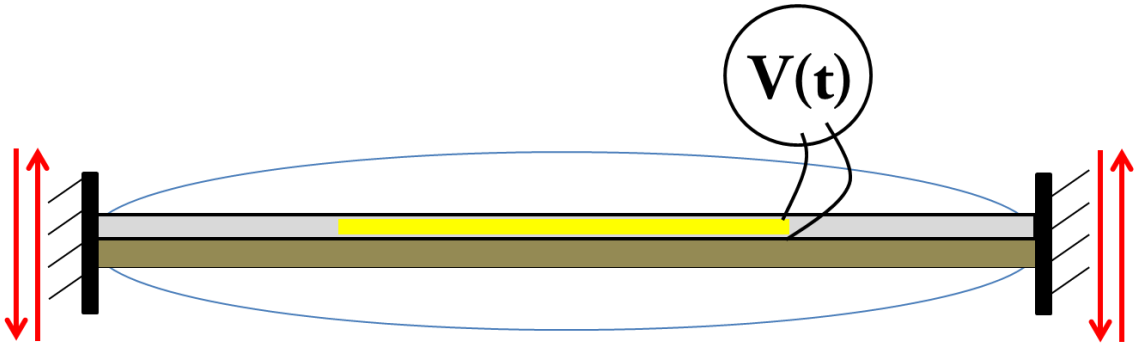

Figure 2: Excited laminated piezoelectric beam actuator driven by an alternating voltage applied to the active area. The reaction forces are shown in red at the clamped boundaries.

The design goal of the actuator is to maximize the vibration transferred to the user. The vibration of the beam can transfer net linear forces or rotational moments to the boundaries. Both reactions can be used to provide haptic user feedback. The current design philosophy is to operate the actuator at resonant frequencies, but the behavior between resonances is also of interest. The following mathematical model and analysis give engineers information about how the actuator's construction affects the design goals outlined above.

Chapter 2

Vibrational Analysis

2.1. Derivation of Equations of Motion

The equations of motion of a system dictate its behavior according to a defined set of variables. For continuous, dynamic systems, these equations are usually high-order partial differential equations. The equation of motion for the system in this study was derived using constitutive equations for piezoelectric materials and Hamilton's Principal.

2.1.1. Constitutive Piezoelectric Equations

Piezoelectricity is the coupling of electric displacement and strain in a material. The relationship between these two quantities is expressed by the piezoelectric equations,

$$D_i = \varepsilon_i^T E_i + d_{iq} T_{qq} \tag{1}$$

$$S_{qq} = d_{iq} E_i + s_{qq}^E T_{qq}$$

where D is the electric displacement, ε^T is electric permittivity under zero stress, E is the electric field, d is the piezoelectric constant, T is the mechanical stress, S is the mechanical strain, and s is the compliance [8]. Piezoelectrics can exhibit significant anisotropic behavior, so the directionality of the constants outlined above are expressed using a subscript system, where "3" indicates the poling direction of the material. In this study the piezoelectric is poled in the z direction. This study is concerned with piezoelectrics designed to operate in the d_{31} regime. For these materials, an electric field applied along the poling direction results in the generation of

strain in the "1" direction, which is the machining direction. The relevant constitutive equations for this case read,

$$D_3 = \varepsilon_3^T E_3 + d_{31} T_{33} \tag{2a}$$

$$S_{33} = d_{31} E_3 + s_{33}^E T_{33} \tag{2b}$$

The piezoelectric beam being studied is voltage-controlled, which means that the electric displacement is known at all times. For this reason, the study focuses on (2)b, which gives the mechanical strain as a function of the electric field and mechanical stress. This behavior is represented below in Figure 3.

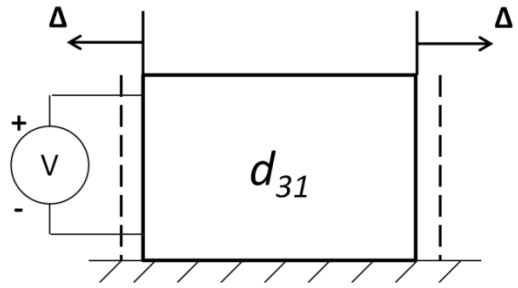

Figure 3: Free expansion (T=0) of a piezoelectric material. The expansion is perpendicular to the electric field and poling direction. d_{31} is a measure of the free strain generated in (*m/V*).

These constitutive equations give a framework for analyzing the effects of active piezoelectric material in the larger system. In the following sections, the equations will be applied in Hamilton's Principal to arrive at the equations of motion for the system.

2.1.2. Analysis of a Piezoelectric Beam

The piezoelectric beam actuator is modeled below with the following parameters,

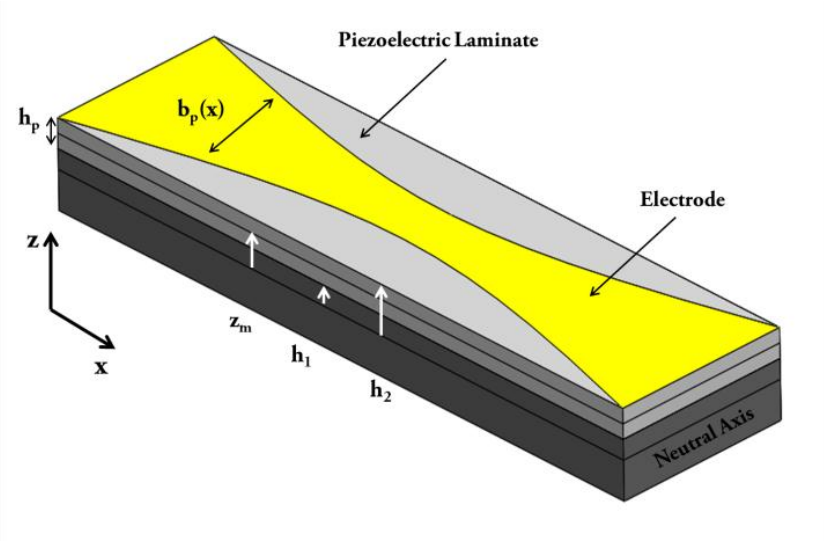

Figure 4: Laminated Piezoelectric Beam with substrate, piezoelectric layer, and shaped electrode. The width of the electrode is defined as $b_p(x)$, and is the only property that varies in the x direction.

where z_m is the distance from the neutral axis to the piezoelectric centerline, $h_1$and h_2 are the heights of the top and bottom of the piezoelectric layer, h_p is the total height of the layer, *l* is the total length of the beam, and $b_p(x)$ is the width of the electrode. The piezoelectric is polarized along the z axis, so that the electric field induced by the voltage on the electrodes produces a strain in the x direction.

The aspect ratio of the laminated beam is assumed to be high, which validates the use of the Euler-Bernoulli assumption. Only transverse displacements, *w(x)*, of the beam are considered and rotations are ignored. Preumont gives a thorough treatment of the laminated piezoelectric beam derivation in his book [9]. The following is a reflection of his process.

Axial strain is related to the beam's curvature by,

$$S_1 = -zw'' \tag{3}$$

The beam's equations of motion are derived using Hamilton's Principle, a variational method that optimizes the definite time integral of the difference between the kinetic and potential energies of a system. It states that,

$$\delta \int_{t_1}^{t_2} (T - V) dt = 0 \tag{4}$$

where δ indicates a virtual displacement, t_1 and t_2 are arbitrary times, T is the kinetic energy, and V is the potential energy. These energies are expressed using generalized coordinates. The method eliminates any internal forces and delivers the equations of motion directly, which makes it attractive for analyzing continuous systems with both electrical and mechanical components. Non-conservative work can be accounted for on the right hand side of the equation, but will not be used because no external forces are assumed.

The kinetic energy for the system is as follows,

$$T = \frac{1}{2} \int_0^l \rho A \dot{w}^2 dx \tag{5}$$

where ρ is the density and A is the cross sectional area. The potential energy of the beam consists of three terms. The first term is the energy stored in the capacitor formed by the upper and lower piezoelectric electrodes; the second term is the piezoelectric energy which arises from the piezoelectric coupling and is dependent on d_{31}; and the third term is the strain energy stored by the deformation of the beam.

$$V = \frac{1}{2} \int_0^l dx \int_A (-\varepsilon_{33} E_3^2 + 2w'' z d_{31} c_{11} E_3 + c_{11} w''^2 z^2) dA \tag{6}$$

Here, ε_{33} is the dielectric constant, E_3 is the applied electric field, d_{31} is the piezoelectric constant, and c_{11} is Young's Modulus. The piezoelectric energy is only present in the active area

of the material, between the upper and lower electrodes. Using this, the second expression can be simplified.

$$\int_A z dA = \int_{h_1}^{h_2} b_p z dz = b_p h_p z_m \tag{7}$$

Also, the last term can be simplified by replacing the integral of Young's modulus and z^2 with *D*, the beam stiffness. This constant is represented as one term instead of the usual *EI* product to avoid confusion with electric constants.

$$D = \int_A c_{11} z^2 dA \tag{8}$$

In some studies, the stiffness of the piezoelectric layer is ignored because its modulus is much lower than that of the substrate. Here, the stiffness of the piezoelectric layer is included because some substrates have moduli close to that of the piezoelectric layer. For the laminated case, the total stiffness of the beam is determined by the stiffness of each material and their relative geometry. The stiffness of each rectangular section about the neutral axis is

$$D = E(\frac{w * h^3}{12} + w * h * {z_m}^2) \tag{9}$$

where *w* is the width, *h* is the height of the section, and z_m is the distance from the section's centroid to the neutral axis. The composite stiffness is the sum of each section's stiffness.

With these substitutions in the piezoelectric and mechanical terms, the potential energy becomes,

$$V = \frac{1}{2}\int_0^l (-\epsilon_{33} E_3^2 + 2w'' e_{31} E_3 b_p h_p z_m + D{w''}^2) dx \tag{10}$$

where e_{31} is $d_{31}c_{11}$. The virtual displacement operator is applied to the kinetic and potential energy expressions for the application of Hamilton's Principle. After integrating by parts, the virtual displacement of the kinetic energy reads,

$$\delta T = \int_0^l \rho A \dot{w} \delta \dot{w} dx = \rho A \dot{w} \delta w]_{t1}^{t2} - \int_0^l \rho A \ddot{w} \delta w dx \tag{11}$$

δw is defined to be zero at t_1 and t_2, so the first term drops out and only the integral is left. The virtual displacement of the potential energy expression reads,

$$\delta V = \int_0^l [e_{31} E_3 b_p h_p z_m \delta w'' + D w'' \delta w''] dx \tag{12}$$

The virtual displacement of the capacitive potential energy term is zero because the system is voltage controlled and the generalized coordinate, *w*, does not appear in the expression. The remaining terms represent the piezoelectric and strain energies. The potential energy expression is further modified by integrating both terms by parts. This procedure isolates terms with *δw*, not its first or second derivative. After integrating by parts, the potential energy is

$$\delta V_e = \left(e_{31} E_3 b_p h_p z_m\right) \delta w']_0^l - \left(e_{31} E_3 b_p h_p z_m\right)' \delta w]_0^l + D w'' \delta w']_0^l + (D w'')' \delta w]_0^l + \int_0^l [\left(e_{31} E_3 b_p h_p z_m\right)'' + (D w'')''] \delta w dx \tag{13}$$

Plugging the virtual displacements for the kinetic and potential energy into Hamilton's Principle yields

$$\int_{t_2}^{t_1} dt \int_0^l [- \rho A \ddot{w} - \left(e_{31} E_3 b_p h_p z_m\right)'' - (D w'')''] \delta w dx - [(\left(e_{31} E_3 b_p h_p z_m\right) + D w'') \delta w']_0^l + [(\left(e_{31} E_3 b_p h_p z_m\right)' + (D w'')') \delta w]_0^l = 0 \tag{14}$$

The first term of the expression must be zero for all admissible virtual displacements, δw. From this, the equation of motion for the system follows.

$$\rho A \ddot{w} + (D w'')'' + \left(e_{31} E_3 b_p h_p z_m\right)'' = 0 \tag{15}$$

Rearranging and collecting constants yields a more useful form of the equation. The left-hand side is the equation of motion for a standard beam. The effects of the piezoelectric layers are captured on the right-hand side as a forcing function.

$$\rho A\ddot{w} + (Dw'')'' = -e_{31}V(t)z_m b_p''(x) \quad (16)$$

The boundary conditions for the system follow from the remaining terms in (13).

$$\delta w'(x) = 0 \;\; || \;\; e_{31}Vz_m b_p(x) + Dw'' = 0 \;\; \begin{cases} x = 0 \\ x = l \end{cases} \quad (17)a$$

$$\delta w(x) = 0 \;\; || \;\; e_{31}Vz_m b'_p(x) + (Dw'')' = 0 \;\; \begin{cases} x = 0 \\ x = l \end{cases} \quad (16)b$$

The first equation creates a moment at the boundary if the rotation of the beam is not prescribed. The second creates a force at the boundary if the displacement at the beam's end is not prescribed. The moment and force at the unconstrained boundaries are proportional to b_p and b'_p, respectively.

2.2. Modal Analysis

The equation of motion for the system is analyzed using the Assumed Modes Method and Galerkin's Method to uncover its dynamic response. These two methods rely on defining test functions to approximate the system. Each test function is multiplied by a generalized coordinate to determine its time dependent magnitude. In this way, the test functions serve as vectors to describe the dynamic behavior of the system.

2.2.1. Assumed Modes Method

The Assumed Modes Method is an approximation that transforms a partial differential equation into a set of ordered differential equations [10]. This creates a discrete approximation of a continuous system that reasonably captures the low frequency behavior.

The transverse displacement of the beam in free vibration is approximated by a series of spatial test functions multiplied by temporal generalized coordinates.

$$w(x,t) = \sum_{i=1}^{\infty} \varphi_i(x) q_i(t) \tag{18}$$

Using this substitution for *w(x,t)* in (16) and assuming free vibration by removing external forcing yields an infinite number of separable PDEs.

$$\rho A \varphi_i(x) \ddot{q}_i(t) + D \varphi_i(x)'''' q_i(t) = 0 \tag{19}$$

Separating by variables produces two ordered differential equations related through the system's natural frequencies, ω_n.

$$\frac{\ddot{q}_i(t)}{q_i(t)} = -\frac{D \varphi_i(x)''''}{\rho A \varphi_i(x)} = \omega_{n_i}^2 \tag{20}$$

The spatial ODE is isolated to identify the modes of the system.

$$\varphi_i''''(x) + \frac{\rho A}{D} \omega_{n_i}^2 \varphi_i(x) = 0 \tag{21}$$

The coefficients in the second term are collected into one parameter,

$$\beta_i^4 = \frac{\rho A}{D} \omega_{n_i}^2 \tag{22}$$

Solving (21), a fourth-order ODE, with the following assumption yields,

$$\text{assume } \varphi_i(x) = A e^{s_i x} \tag{23a}$$

$$\varphi_i(x) = C_1 cosh(\beta_i x) + C_2 sinh(\beta_i x) + C_3 cos(\beta_i x) + C_4 sin(\beta_i x) \tag{23b}$$

The application of the boundary conditions determine the specific shape functions used to approximate the system. For a clamped-clamped beam, the rotation and displacement at both ends are fixed at zero. All modes for the system must meet these criteria.

$$\begin{matrix}\varphi_i(0)=0\\ \varphi'_i(0)=0\\ \varphi_i(l)=0\\ \varphi'_i(l)=0\end{matrix} \tag{24}$$

Applying all four boundary conditions creates a system of equations that simplifies to,

$$1-\cosh(\beta_i l)\cos(\beta_i l)=0 \tag{25}$$

The infinite values of β_i that solve this equation are unique to a clamped-clamped beam. The four constants in (23)b can be consolidated into one constant, α_i.

$$\varphi_i(x)=sin(\beta_i x)-\sinh(\beta_i x)+\alpha_i\big(\cos(\beta_i x)-cosh(\beta_i x)\big) \tag{26}$$

These test functions form an orthogonal set that can be used to describe the state of the system. In order to make the set orthonormal, a constant c_i is added by integrating the functions over the length of the beam. Traditionally, the modes would be mass normalized, but inclusion of the mass is not necessary because it is assumed not to vary in the x direction.

$$c_i\int_0^l \varphi_i(x)dx=1 \tag{27}$$

The modes of a clamped-clamped beam are described as,

$$\varphi_i(x)=c_i\big[sin(\beta_i x)-\sinh(\beta_i x)+\alpha_i\big(\cos(\beta_i x)-cosh(\beta_i x)\big)\big] \tag{28a}$$

$$\text{where}\quad \alpha_i=\frac{\sin(\beta_i l)-\sin\mathrm{h}(\beta_i l)}{\cos(\beta_i l)-\cosh(\beta_i l)} \tag{28b}$$

These modes are orthonormal vectors that are used to describe the shape of the system at any time. Technically, any set of functions could have been used as the test functions of the system. The modes are advantageous as test functions because they are orthonormal. This property is a requirement for Galerkin's Method, which will determine the time dependent generalized coordinate associated with each mode.

2.2.2. Galerkin's Method

Galerkin's Method is common weighted residual method [10]. The method is used to derive approximate solutions to differential equations. To start, *w(x,t)* is assumed to be the sum of the product of a set of orthonormal test functions (the modes) and a time dependent generalized coordinate, as in (18). When only a finite number of test functions is used, there will be some behavior not captured by this sum. This error is called the residual, *R*. Substituting (18) into the equation of motion (16) and rearranging yields,

$$\sum_{i=1}^{n} \rho A \ddot{q}_i \varphi_n + \sum_{i=1}^{n} D q_i {\varphi_n}'''' + e_{31} V z_m b_p''(x) = R \tag{29}$$

Next, (29) is multiplied by φ_m and integrated over the length of the beam.

$$\sum_{i=1}^{n} \rho A \ddot{q}_n \int_0^l \varphi_n \varphi_m dx + \sum_{i=1}^{n} D q_n \int_0^l \varphi_n'''' \varphi_m dx + e_{31} V z_m \int_0^l {b_p}''(x) \varphi_m dx \tag{30}$$

$$= \int_0^l R \varphi_m dx$$

Equation (30) can be simplified using,

$$\sum_{i=1}^{n} \int_0^l \varphi_n \varphi_m dx = \delta_{nm} \tag{31a}$$

$$\sum_{i=1}^{n} \int_0^l \varphi_n'''' \varphi_m dx = \sum_{i=1}^{n} \int_0^l \beta^4 \varphi_n \varphi_m dx = \beta^4 \delta_{nm} \tag{31b}$$

$$\omega_n^2 = \frac{D\beta^4}{\rho A} \tag{31c}$$

The equation below is the actuator equation. It governs the response of each mode. Again, the piezoelectric contribution can be seen as a forcing function on the right hand side. The difference in forcing from mode to mode is dependent only on the integral of the second derivative of the active area width and the normalized mode shape. This fact becomes very

important when comparing the amount of forcing different active area profiles impart on the system.

$$\ddot{q}_n + {\omega_n}^2 q_n = -\frac{e_{31} V(t) z_m}{\rho A} \int_0^l b_p''(x)\, \varphi_n dx \tag{32}$$

2.2.3. Frequency Response

A frequency response is the measure of the output of a system normalized to the stimulus [10]. For the clamped-clamped beam, the output is the set of q_n and the input is the voltage. If the input voltage is assumed to be sinusoidal, equation (32) can be solved as the following,

$$q_n = Q_n e^{i\omega t} \tag{33a}$$

$$Q_n(\omega) = -\frac{e_{31} V_{amp} z_m}{\rho A(\omega^2 - {\omega_n}^2)} \int_0^l b_p''(x)\, \varphi_n dx \tag{33b}$$

It is useful to categorize the response of the system to the driving input with a dimensionless quantity. This quantity is *H*, the frequency response.

$$H_n(\omega) = \frac{Q_n}{V_{amp}} \tag{34}$$

The frequency response is a function of the driving frequency. The total response of the beam at any x-coordinate is the sum of the mode shapes multiplied by the corresponding frequency response.

$$X(\omega, x_o) = \sum_{i=1}^{n} H_n(\omega)\varphi(x_o) \tag{35}$$

This is useful for calculating the net reaction force and moment in the following section.

2.2.4. Reaction Forces and Moments

The goal of the actuators being studied is to transfer vibrational energy to the user through the system's boundary condition. The amplitude of the net normalized reaction force and moment are used to characterize what the user will feel when the device is in operation. Normalizing the reactions to the input voltage make it easier to apply simulation results to multiple cases.

The net normalized reaction force amplitude follows from Newton's first law. The voltage normalized force for a single particle in the beam is,

$$\frac{F(\omega,x)}{V} = -m\omega^2 A(\omega,x)\cos(\omega t) \tag{36}$$

$$\text{where} \quad A(\omega,x) = \sum_{i=1}^{n} H_i(\omega)\varphi_i(x)$$

The amplitude of this force is

$$F_{amp}(\omega) = m\omega^2 A(\omega,x_o) \tag{37}$$

Equation (37) is extended to the continuous system by integrating along the length of the beam.

$$F_{amp}(\omega) = \sum_{i=1}^{n}\int_0^l \rho A\omega^2 H_i(\omega)\varphi_i(x)dx \tag{38}$$

This expression gives the amplitude of the normalized reaction force transferred from the vibrating beam into the boundary conditions. The net normalized moment is derived in a similar manner. The moment caused by a single particle about the mid-length of the beam is,

$$M = Fx \tag{39}$$

Using equation (39), the voltage normalized moment amplitude about the mid-length of the beam is,

$$M_{amp} = \sum_{i=1}^{n} \int_{\frac{l}{2}}^{\frac{l}{2}} \rho A \omega^2 H_i(\omega) \varphi_i \left(x + \frac{l}{2}\right) x dx \quad (40)$$

This gives the voltage normalized moment transferred to the boundary conditions by the system. The net voltage normalized force and moment are used to characterize actuator's effectiveness.

2.2.5. Case Selection

Based on the preceding analysis, two cases for the active area shape were deemed interesting and chosen for study. The first case is that of a "patch actuator." The active area was assumed to be rectangular, with the width equal to the width of the beam and the length determined by start and end positions, *a* and *b*.

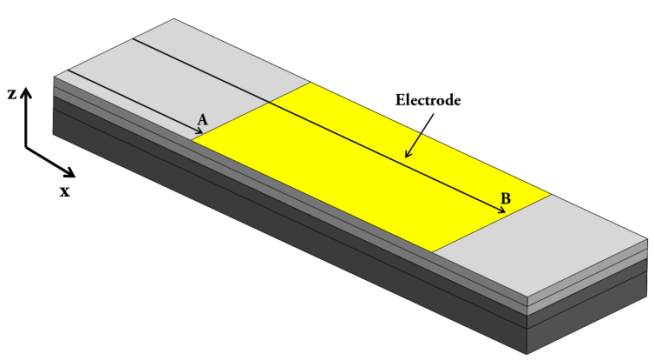

Figure 5: The patch actuator case, representing the current design configuration. The electrode is a rectangle of width equal to the beam with start and end positions designated by *a* and *b*.

The active area patch can be described using the Heaviside function. The modal forcing of the profile is determined by its second derivative. The second derivative of the Heaviside function is the first derivative of the Dirac delta function, δ'.

$$b(x) = H(x-a) - H(x-b) \quad (41)a$$

$$b''(x) = \delta'(x-a) - \delta'(x-b) \quad (41)b$$

Under an integral, the Dirac delta isolates specific values of the functions it is multiplied with, which can be proven using integration by parts. This behavior is described below,

$$\int_0^l \delta^{(n)}(x - x_0) f(x) dx = (-1)^n f^{(n)}(x) \tag{42}$$

Using equation (41)b and the integral of the modal forcing equation (32),

$$\int_0^l b''(x)\, \varphi_n(x) dx = \int_0^l [\delta'(x - a) - \delta'(x - b)] \varphi_n(x) = \varphi_n{}'(b) - \varphi_n{}'(a) \tag{43}$$

Equation (43) shows that a discontinuous, patch shaped active area excites each mode based on the values of the first derivative of the mode shape at the start and end of the patch. In the analysis, two patches were used to maximize (43) for modes 1 and 2.

$$\text{Mode 1: } a = .2242 \quad b = .7758 \tag{44}$$

$$\text{Mode 2: } a = .1321 \quad b = .5000$$

The second case involves tailoring the active area to excite specific modes of the beam as suggested in the work of Lee and Moon. The integral of the modal forcing equation (32) provides the motivation behind this method.

$$\int_0^l b_p{}''(x)\, \varphi_n dx \tag{45}$$

By judiciously choosing b_p, we can ensure that the active area only excites one specific mode and maximized the integral.

$$b_p(x) = \varphi_p{}'' \tag{46}$$

$$\int_0^l b_p{}''(x)\, \varphi_n dx = \int_0^l \varphi_p{}''''\, \varphi_n dx = \beta_p^4 \delta_{pn}$$

2.3. Numerical Simulation

The equations derived in the sections above were analyzed using two computational programs, Mathematica and MATLAB. These numerical simulations produced performance data used to compare the patch actuator and the modal actuator cases. This section describes the numerical simulation process.

Mathematica is powerful computational software that is particularly useful for symbolic algebra [10]. The symbolic algebra package was used to apply the clamped-clamped boundary conditions (24) to the general mode shape equation (23)b, yielding equation (25). This was solved for the first ten values of β_i. These values were then fed to the MATLAB script for further calculations.

MATLAB is a high-performance language for technical computing [11]. The script used to analyze the clamped-clamped beam is broken up into sequential cells. The order and specific equations for each cell is outlined below.

Table 1 Outline of the MATLAB code used to numerically simulate the performance of the laminated clamped-clamped piezoelectric beam. The name, function, and pertininent equations for each cell is listed.

Cell	Function
Mechanical Properties and Dimensions	Define geometry of beam, modulus, and density of beam
Electric Properties	Define Piezoelectric constants, voltage, and active area
Composite Beam	Solve equation (9) for composite stiffness
Natural Frequencies and Mode Shapes	Use list of β_i from Mathematica to solve equations (28)b, (27), and (31)c
Frequency Response	Solve for the modal forcing (33)b, modal frequency response (34) and the total response (35)
Net Reaction Force and Moment	Solve equations (38) and (40) for the net reaction force and moment amplitude

The geometric, material, and electric properties of the laminated beam were chosen to represent a general actuator case and do not reflect the parameters of a single device. The relevant properties used in the analysis are as follows,

Table 2 Parameters used to define the clamped-clamped laminated piezoelectric beam in the numerical analysis. These parameters include material properties, electric properties, and geometry.

Piezoelectric Layer		Substrate Layer	
Density	1700 kg/m^3	Density	1350 kg/m^3
Young's Modulus	.6e9 Pa	Young's Modulus	3.38e9 Pa
Height	.0005 m	Height	.0005 m
Width	.0100 m	Width	.0100 m
Length	.3000 m	Length	.3000 m
d_{31}	10.4 m/V		
V	200V		

The first five modes were used to approximate the behavior of the system. The analysis was truncated at five for several reasons. The first is that the assumed modes method is a low frequency approximation and the contributions of higher modes will be reduced by viscoelastic damping. In addition, the operating bandwidth of the device is assumed to be below the third mode, which makes response information at high frequencies unnecessary.

The integrals in the last two cells were calculated using the "quad" function in MATLAB. This function numerically integrates user-defined functions using Simpson quadrature [11]. The tolerance was set to 1.0e-6, but this still produced noticeable errors in some results. The identification and handling of these errors is discussed in the results section.

The natural frequencies, frequency response, and reaction force and moment amplitude were the crucial results of this analysis. These data sets serve as metrics with which the cases outlined in the previous section are compared. All plots were made using MATLAB.

Chapter 3

Results and Discussion

The results presented below were produced using theoretical modeling and numerical simulations for a clamped-clamped, laminated piezoelectric beam. The most pertinent findings were the natural frequencies, mode shapes, and various force and moment responses for the system. The results of the two cases chosen for study are presented and compared below.

3.1. Mode shapes and Natural Frequencies

The normalized modes of the system as described by equation (28)a were generated by a user-defined function in MATLAB. The first three modes of the system are plotted below.

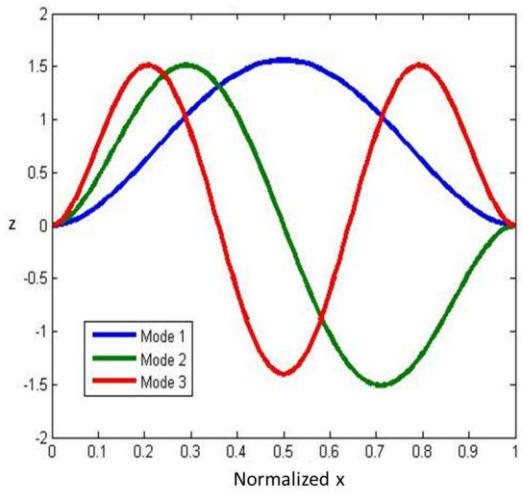

Figure 6: First three normalized mode shapes of a clamped-clamped beam. Odd mode shapes are always symmetric about the mid-length of the beam. Even modes are rotationally symmetric about the mid-length of the beam.

More humps develop as the mode number gets higher. Two important trends emerge; The odd mode shapes are all symmetric about the mid-length of the beam, making it impossible for

odd modes to generate a moment about the mid-length; and even modes are rotationally symmetric about the mid-length, making it impossible for them to generate a net force. These facts will be used in the following sections to address computational error. Each of the modes resonate at a specific natural frequency defined by equation (31)c. The natural frequencies of the first five modes are as follows,

Table 3 Natural Frequencies of the first five modes of the laminated piezoelectric beam. The natural frequencies are dependent on β_i, D, ρ, and A.

Mode 1	Mode 2	Mode 3	Mode 4	Mode 5
74.83 Hz	206.28 Hz	404.39 Hz	668.49 Hz	998.61 Hz

3.2 Discontinuous Patch Actuators

Two discontinuous piezoelectric patch actuators were the first cases studied. The start and end positions of the patches were chosen to maximize the forcing on the first and second modes, respectively. The five modal frequency response functions for the mode 1 patch actuator are shown in Figure 7. The patch was placed symmetrically about the mid-length of the beam. This explains why the symmetric, odd modes (1,3,5) have much higher responses than the asymmetric, even ones (2,4). The peaks of the five response functions correspond to the natural frequencies in Table 2.

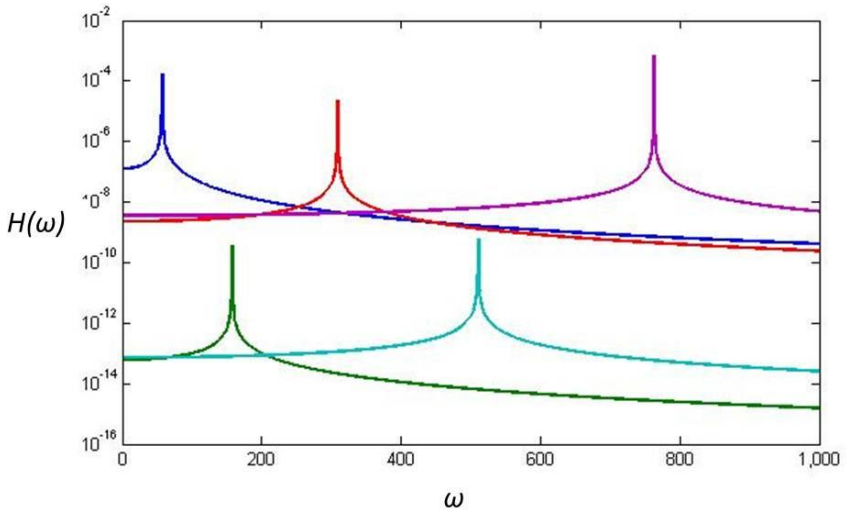

Figure 7: Modal frequency response functions for the first five modes of the mode 1 patch actuator. The response functions, H_i, are the generalized coordinates that determine the response of each mode across the range of frequencies.

The net reaction force from equation (38) for the two patch cases is shown in Figure 8. As expected, the symmetric odd modes show the greatest force amplitude. The patch designed to maximize the force for mode 1 had the greater response at the first natural frequency. Interestingly, the response for the same actuator at the fifth mode was even greater than the first mode. This occurred because the force is proportional to ω^2, but this response would be tempered by structural damping if that factor was included. Also of note is the fact that the asymmetrically placed mode 2 actuator still excited the odd modes and produced at least some force.

The net reaction moment from equation (40) for the two patch cases is shown in Figure 9. Here the even modes produced the greatest response; the peaks are clear at the natural frequencies for modes 1 and 2. The symmetrically placed mode 1 patch did not induce an appreciable moment at any frequency.

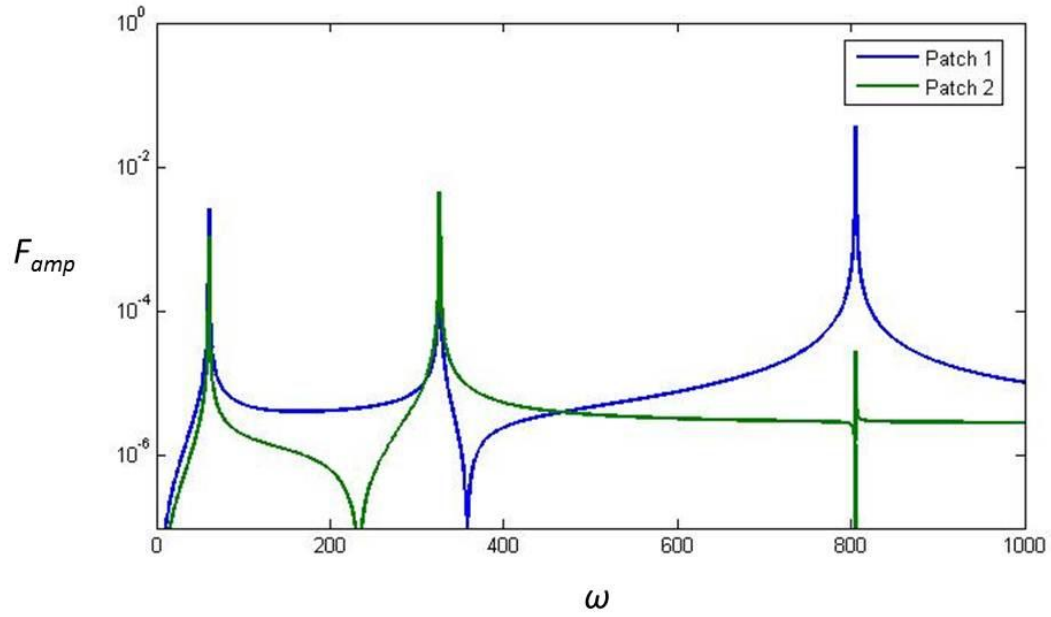

Figure 8: Net normalized reaction force amplitude for the two patch cases. The odd modes (1,3,5) show high responses at their respective resonant frequencies. As predicted, there is no appreciable net force response from the even modes.

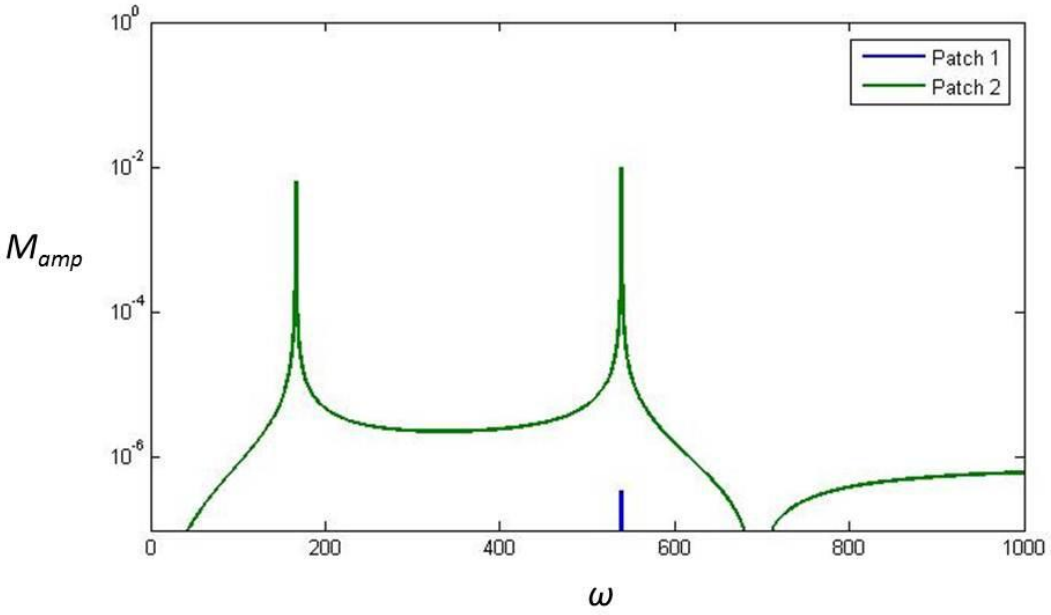

Figure 9: Net normalized reaction moment amplitude for the two patch cases. The asymmetric mode 2 patch actuator produces peaks at the resonant frequencies for modes 2 and 4. The symmetric mode 1 patch actuator does not produce an appreciable moment at any mode. The small peak at the mode 4 resonant frequency is a result of errors in the numerical integration process.

The moment and especially the force analysis shown above demonstrate the interesting vibrational behavior that can be excited by patch actuators. In general, such varying response, with distinct peaks and troughs is not very useful for actuator design. Peaks can be used to transfer vibrations at specific frequencies, but in between those resonances a more predictable and flat response is desired.

3.3 Modal Actuators

The two modal actuators chosen for simulation were shaped to excite the first two modes of the beam. The net reaction force amplitude of the modal actuators is shown in Figure 10 against the results from the patch cases. As expected, the mode 1 modal actuator produces significantly higher reaction force amplitude compared to the patch actuators. The modal forcing for the modal actuator was 17.65 times larger than the mode 1 patch actuator. In addition, the response is higher almost across the entire frequency range and is flat away from the first resonance. The patch actuators only produce a larger force at modes three and five where they can resonate but the modal actuators cannot. Again, this apparent advantage would be flattened out by damping if it was included in the model.

The moment amplitude results for the mode 2 modal actuator are also a large improvement on the two patch actuator cases. The modal forcing produced by the modal actuator is 25.49 times greater than the patch actuator. Again, the moments produced by the shaped active area are significantly higher across the frequency range and the off-resonance response is flat. The mode 2 patch actuator does produce a higher moment at the mode 4 natural frequency.

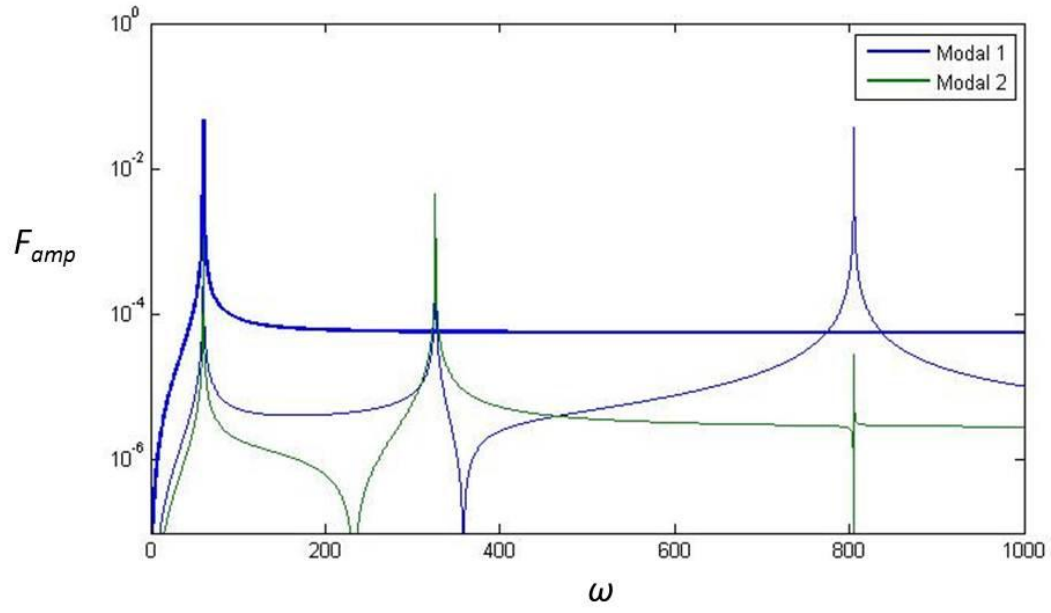

Figure 10: Net reaction force amplitude of modal actuators plotted against the patch actuators for comparison. The 1st modal actuator produces forcing 17.65 times greater than the patch actuator for the 1st mode. The modal actuator for the 2nd mode does not produce any net force.

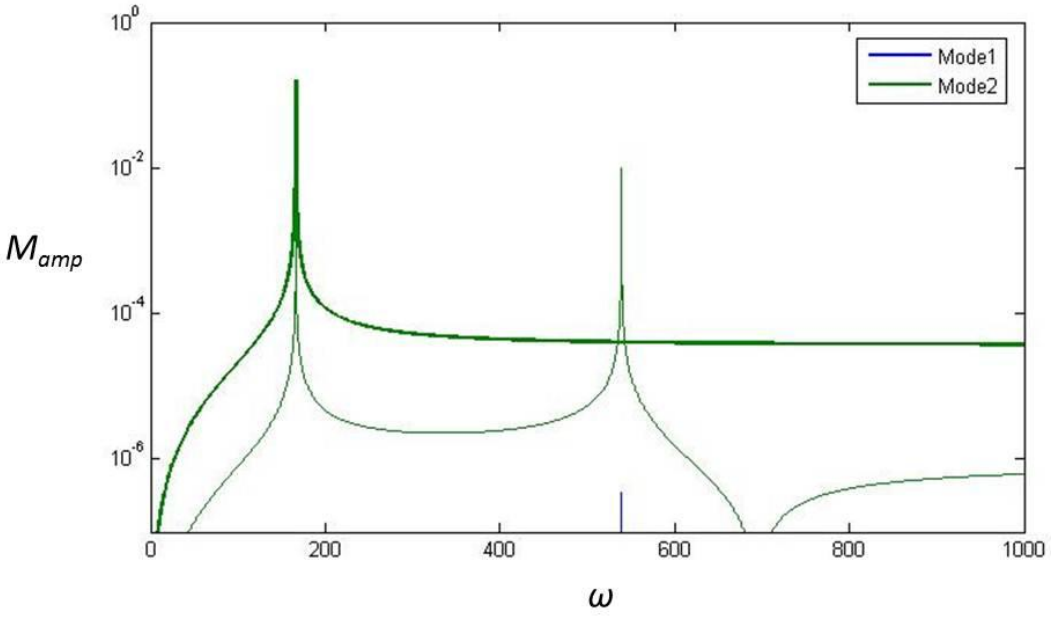

Figure 11: Net reaction moment amplitude of modal actuators plotted against the patch actuators for comparison. The 2nd modal actuator produces forcing 25.49 times greater than the patch actuator for the 2nd mode. The modal actuator for the 1st mode does not produce any net moment.

Chapter 4

Conclusions & Future Work

Based on the results outlined above, it is clear that modal actuators with tailored active area geometry are more effective at driving a clamped-clamped piezoelectric beam than the patch geometry currently being used. The force and moment plots in the preceding figures paint a clear argument for this. The modal actuators produce stronger vibrational forces and moments across the range of frequencies up to the third mode. In addition, the response of the modal actuators is flat away from the resonant peaks. This uniformity is much more useful from a design perspective than the response produced by the patch actuators. The patch actuators only produce stronger reactions at the higher modal resonances (3,4,5). These apparent advantages are not useful. Structural damping will flatten out the response at higher frequencies, and higher modes will in all likelihood resonate out of the useful haptic range for a realistically sized device.

The results of this study have significant impacts on the design methodology for constructing laminated piezoelectric beam actuators. The most pressing is that the beam actuators being prototyped at SPS should use the tailored active area geometry defined in equation (46) to create modal actuators. This should be a relatively small departure from the current construction technique. Two major changes in the process need to be made. First, a layer of piezoelectric needs to be added to the bottom of the beam, creating a double layer laminated beam. The electrodes on the bottom piezoelectric layer will match the negative portions of the second derivative of the mode shape. Second, the masks used to determine the electrode geometry need to be shaped according to the positive and negative parts of (46) and scaled to fit the width of the actuators. These two simple steps will allow the engineers to make modal actuators and increase the force and moment vibrations their devices can generate. They can then use the stronger vibrations to better transmit haptic information to the user.

This study is also useful as a learning tool for the design process. The work presented here utilized well established analysis techniques like Hamilton's Principal, the Assumed Modes Method, and Galerkin's Method to derive the equations that govern the behavior of the laminated piezoelectric beam. This theoretically-based approach yielded significant design insights that would not have been obvious if other methods were used. The most important insights stem from equations (28)a and (32). Plots of the mode shapes generated from (28)a make it clear that odd and even modes make the system react in very different ways. One transmits net forces to the user, while the other transmits net moments. This result opens up two types of tactile information that the actuator can convey. Equation (32) shows that the forcing imparted to each mode depends only on the active area profile's second derivative and how closely it matches each mode shape. This conclusion is not self-evident, and would not be obvious without the equations derived from the theoretical approach. Currently, actuator behavior is predicted using large, expensive Finite Element Analysis (FEA) packages. These detailed, mesh-based analyses are invaluable for specific design cases, but they do not evince overarching system properties. The results of this study did not include the same level of detail that the FEA approach could have, but are results applicable to a wide variety of cases as opposed to just one. The model can be easily changed to account for other types of beam boundary conditions, geometry, and mass distributions. The insights and versatility that the theoretically-based analysis provide make it a valuable design too that should be used in conjunction with FEA packages to predict actuator performance.

The results and conclusions of this study point to several areas of future work. The most important is actually building a modal actuator as described above and evaluating its performance versus the patch actuators and actuators available commercially. This analysis did not account for several factors that may make the system's physical response differ from the predicted response. These factors include the assumption that the beam's piezoelectric layer is a bulk material and that it behaves linearly. The Euler-Bernoulli assumption may also not hold if the beam aspect

ratio becomes smaller. Lastly, damping was not included in the model. Building and testing an actuator similar to the one analyzed in this study will show which of these assumptions hold for the physical system. Using that information, the accuracy of the model can be improved.

The second thrust of future work should focus on the haptic performance of the actuator. Other methods for increasing the reaction forces and moments produced by the system should be investigated. These include adding mass to the beam and changing the boundary conditions of the system. The changes can be evaluated using the mathematical model before constructing a physical actuator. Lastly, it would be interesting to assess the effectiveness of using net forces to transfer haptic information versus net moments. The user should be able to feel the difference between these two reactions. A study should be conducted to assess the responses each one elicits in users. It's possible that each type of reaction is more effective at communicating certain types of information.

REFERENCES

[1] Leung, R., MacLean, K., Bertelsen, M., & Saubhasik, M. (2007, November). Evaluation of haptically augmented touchscreen gui elements under cognitive load. *International conference on multimodal interfaces*, Nagoya, Japan.

[2] Levin, M., & Woo, A. (2009). Tactile-feedback solutions for an enhanced user experience. *Information Display*, 18-21.

[3] Haptics in touch screen hand-help devices. (2012). *Immersion Corporation Whitepaper*

[4] Ballas, R. G. (2007). Piezoelectric multilayer beam bending actuators. (pp. 17-26). Berlin: Springer.

[5] Ueberschlag, P. (2001). PVDF piezoelectric polymer. *Sensor Review, 21*(2), 118-125.

[6] Lee, C. K., & Moon, F. C. (1990). Modal sensors and actuators. *Journal of Applied Mechanics, 57*, 434-441.

[7] Aldraihem, O. J., Wetherhold, R. C., & Singh, T. (1997). Distributed control of laminated beams: Timoshenko theory vs. euler-bernoulli theory. *Journal of intelligent Material Systems and Structures, 8*(2), 149-157.

[8] IEEE standard on piezoelectricity. (1988). New York, NY: The Institute of Electrical and Electronics Engineers, Inc.

[9] Preumont, A. (2006). Mechatronics: Dynamics of electromechanical and piezoelectric systems. (pp. 1-39;95-156). Netherlands: Springer.

[10] Meirovitch, L. (2000). Principles and techniques of vibrations. (pp. 74-96; 518-548). New York: Prentice-Hall.

[10] Mathematica Documentation. (2013). Wolfram.

[11] MATLAB Documentation. (2013). The MathWorks, Inc.

Appendix A

Matlab Code

```
%% Mechanical Props/Dims of [Piezoelectric, Substrate]
density = [1700,1350]; %[kg/m^3]
E = [.600e9,3.38e9];    %[pa]
height = [.0005,.001]; %m
width = .01;
L = .5;
mass = density.*height*width*L;

%% Electric Properties
d31=10.4; %e-12 strain/(V/m)
V=200; %V
e31=d31*10e-12*E(1);
continuousflag = 1;
if continuousflag
    mode = 2;
else
activebound = [.1321,.5000]; %Normalized [START, END] of Strip
end

%% Composite Beam
neutralaxis = (height(2)*(E(2)*height(2)*width+...
2*E(1)*height(1)*width)-height(1)*E(1)*height(1)*width) ...
/2/(E(2)*height(2)*width+E(1)*height(1)*width);
c = [height(2)+height(1)/2-neutralaxis,neutralaxis-height(2)/2];
clear stiffness
stiffness=0;
for i = 1:2
 stiffness = stiffness +
E(i)*(width*height(i)^3/12+width*height(i)*c(i)^2);
end
zm = c(1);

%% Nat. Freqs & Mode Shapes
betallist = [4.73004, 7.8532, 10.9956, 14.1372, 17.2788, 20.4204,
23.5619,...
    26.7035, 29.8451, 32.9867]; %from mathematica

for ii = 1:length(betallist)
alphalist(ii) = (sin(betallist(ii))-
sinh(betallist(ii)))/(cos(betallist(ii))...
    -cosh(betallist(ii)));
end

%C's are NOT mass normalized b/c mass does not varry with x
for ii = 1:length(betallist)
clist(ii)=1/quad(@ClampClampModeShapeSqrd,0,1,0.000001,0,[betallist(ii)
,alphalist(ii)]);
end
```

```
for ii = 1:length(betallist)
    wnat(ii)=betallist(ii)^2*sqrt(stiffness/sum(mass)/L^4);
end

%% Freq Response
%Integrate Forcing Function*Modes
clear modalforcing
if continuousflag
    modalforcing = zeros(1,10);
    modalforcing(mode)= -
e31*zm*width/ClampClampModeShapePrime2(0,[betallist(mode),alphalist(mod
e)])*(betallist(mode)/L)^4;
else
    for ii = 1:length(betallist)
        modalforcing(ii) = -
e31*zm*width*(ClampClampModeShapePrime(activebound(1),[betallist(ii),al
phalist(ii)])-...

ClampClampModeShapePrime(activebound(2),[betallist(ii),alphalist(ii)]))
;
    end
end
%Calculale Response Magnitude for each mode
w=1:.1:1000;
clear Q H
for ii = 1:length(betallist)
    for jj = 1:length(w)
    Q(ii,jj) = modalforcing(ii)*V/sum(mass)/(wnat(ii)^2-w(jj)^2);
    H(ii,jj) = Q(ii,jj)/V;
    end
end
modenumbers = [1,2,3,4,5];
x = 0:.01:1;
clear freqresponse
for xx = 1:length(x)
    for jj = 1:length(w)
        sumsum = 0;
        for ii = 1:length(modenumbers)
            sumsum = sumsum +
H(modenumbers(ii),jj).*ClampClampModeShape(x(xx),[betallist(modenumbers
(ii)),alphalist(modenumbers(ii))]);
        end
        freqresponse(xx,jj)= sumsum;
    end
end

%% Integrate for Net Reaction Force and Moment
clear reactionforce
reactionforce = zeros(1,length(w));
for jj = 1:length(w)
    for ii = 1:length(modenumbers)
```

```
        reactionforce(jj) =
reactionforce(jj)+sum(mass)*w(jj)^2*H(modenumbers(ii),jj)*L*clist(ii)*q
uad(@ClampClampModeShape,0,1,0.000001,0,[betallist(ii),alphalist(ii)]);
    end
end
clear reactionmoment
reactionmoment = zeros(1,length(w));
for jj = 1:length(w)
    for ii = 1:length(modenumbers)
        reactionmoment(jj) =
reactionmoment(jj)+sum(mass)*w(jj)^2*H(modenumbers(ii),jj)*L*clist(ii)*
quad(@ClampClampModeShapeMoment,-
.5,.5,0.000001,0,[betallist(ii),alphalist(ii)]);
    end
end


--

function [U] = ClampClampModeShape(x,param)
U = (sin(param(1)*x)-sinh(param(1)*x))...
    -param(2)*(cos(param(1)*x)-cosh(param(1)*x));
end

--

function [Uprime] = ClampClampModeShapePrime(x,param)
Uprime = param(1)*(cos(param(1)*x)-cosh(param(1)*x))...
    + param(1)*param(2)*(sin(param(1)*x)+sinh(param(1)*x));
end

--

function [Usqrd] = ClampClampModeShapeSqrd(x,param)
U = ((sin(param(1)*x)-sinh(param(1)*x))...
    -param(2)*(cos(param(1)*x)...
    -cosh(param(1)*x)));
Usqrd=power(U,2);
end
```

ACADEMIC VITA

Joseph Giordano

Jag5519@psu.edu

Education

Bachelor of Science Degree in Engineering Science, Honors Curriculum
The Pennsylvania State University
The Schreyer Honors College
Engineering Leadership Development Minor
Graduation Date: May, 2013
Thesis Title: Vibrational Modeling of a Laminated Piezoelectric Beam for Frequency Response Predictions
Thesis Supervisor: Dr. Joseph Cusumano

Experience

Design, Analysis, and Fabrication for Commercialization of Piezoelectric Actuators
Strategic Polymers Inc., State College
Summer 2012-Present

- Thrived in a Tech Startup, results focused atmosphere
- Designed prototypes, lab equipment, and circuit layouts using SolidWorks
- Fabricated and assembled prototypes, electronics, and machinery

Turbofan Engine Low Pressure Turbine Vane Cluster Analysis
Pratt & Whitney, East Hartford
Fall 2011

- Repaired, parameterized and meshed complex geometry in SolidWorks and ANSYS
- Identified five high stress areas prone to fatigue failure using Finite Element Analysis
- Coordinated with Singaporean engineering students to meet customer needs

Mushroom Agricultural Development in the Gaza Strip
Engineering Leadership Development Minor, State College
Spring 2010

- Lead an international team of students from PSU, Hungary, and Gaza
- Presented research findings to the Department of Agriculture of Gaza

Particle Shadow Velocimetry: System Evaluation, Calibration, and Refinement
Applied Research Laboratory, State College
Summer 2010

- Improved data acquisition process using high-speed image capture equipment
- Created MATLAB code to correct for Geometric Distortion and Color Crosstalk

Honors and Awards

Schreyer Honors College Scholarship
Leonhard Engineering Honors Scholarship
Joseph Marin Memorial Scholarship
President's Freshman Award
Dean's List

Association Memberships/Activities

Penn State Blue Band
Guide, 2012-2013
Member, 2009-2012
Springfield THON
Canning Chair, 2010-2011
Member 2009, 2011-2013
Teaching Intern, Engineering Leadership Development Minor
Introduction to Leadership, 2013